Hayabusa 2 returned samples reveal a weak to null magnetic field during aqueous alteration of Ryugu's parent body

C. Maurel, Jérôme Gattacceca, Minoru Uehara

Earth Planet. Sci. Lett. 627 (2024) 118559

Contents lists available at ScienceDirect

Earth and Planetary Science Letters

journal homepage: www.elsevier.com/locate/epsl

Hayabusa 2 returned samples reveal a weak to null magnetic field during aqueous alteration of Ryugu's parent body

C. Maurel *, J. Gattacceca, M. Uehara

CNRS, Aix Marseille Univ, IRD, INRAE, CEREGE, Aix-en-Provence, France

ARTICLE INFO

Edited by Dr. F. Moynier

Keywords:
Paleomagnetism
Hayabusa 2
Ryugu
Aqueous alteration
Solar nebula
Magnetic field

ABSTRACT

The JAXA Hayabusa 2 mission returned 5.4 g of material from the C-type asteroid Ryugu. The Mn-Cr ages of dolomite in the returned samples indicate that Ryugu's parent body experienced aqueous alteration sometimes between <1.8 and 6.8 Myr after CAI formation. Because this time range overlaps with the lifetime of the solar nebula, we investigate the possibility that magnetite and pyrrhotite, which are aqueous alteration products found in Ryugu samples, acquired a remanent magnetization reflecting the nebula field intensity. We analyze the intrinsic magnetic properties and paleomagnetic record of three Ryugu samples of 0.82, 0.97 and 21.87 mg. None of the samples exhibit a stable natural remanent magnetization. This indicates that the aqueous alteration of Ryugu's parent body took place either in a field of a few μT, or in a very weak to null field. In the former scenario, the solar nebula field is the most likely magnetizing field, implying that aqueous alteration occurred before its dissipation, i.e., before ~5 Myr after CAI formation. In the latter scenario, aqueous alteration must have occurred either after the dissipation of the nebula, or at an earlier epoch and a large heliocentric distance (> 5 au). The similarities between Ryugu samples and CI chondrites favor this second hypothesis. Our results contrast with another paleomagnetic study of two Ryugu samples, arguing for a paleofield intensity of 40 to 390 μT. Our interpretation of this discrepancy is that these samples were exposed to artificial magnetic fields (> mT) during preceding experiments. This highlights the importance of conducting, as much as possible, the paleomagnetic investigations of returned samples before any other experiment. We also demonstrate that the ratio of NRM over low-field magnetic susceptibility is a powerful, non-destructive indicator of magnetic contamination. We recommend measuring this ratio routinely before paleomagnetic investigations of meteorites and returned samples.

1. Introduction

The JAXA Hayabusa 2 mission returned to Earth 5.4 g of material from the surface of the C-type asteroid Ryugu (Watanabe et al., 2019; Yada et al., 2021). The collected samples are similar to CI chondrites in mineralogy, chemical composition and isotopic composition (Nakamura et al., 2022; Yokoyama et al., 2023). The parent body of Ryugu, like that of the CI chondrites, may have formed in a separate and more distant region of the solar nebula compared to most carbonaceous chondrites (Desch et al., 2018; Hopp et al., 2022). The mineralogy of returned samples, in particular their abundant phyllosilicates, dolomite, magnetite and pyrrhotite, reflects an extensive aqueous alteration on Ryugu's parent body (Nakamura et al., 2022).

The formation of dolomite can be dated using the ^{53}Mn-^{53}Cr isotopic system to infer the age of aqueous alteration. Two studies found significantly different results. On the one hand, Yokoyama et al. (2023) concluded that aqueous alteration occurred sometimes between 3.1 and 6.8 million years (Myr) after the formation of calcium aluminum rich inclusions (CAIs), given the uncertainties on the initial ^{53}Mn-^{53}Cr ratio. On the other hand, McCain et al. (2023) obtained an upper limit of 1.8 Myr after CAI formation, using different standards to derive the initial ^{53}Mn-^{53}Cr ratio.

This estimated range of aqueous alteration ages (between < 1.8 and 6.8 Myr after CAI formation) overlaps with the lifetime of the solar nebula, which dissipated ~5 Myr after CAI formation (Wang et al., 2017). Paleomagnetic studies show that magnetic fields were present in the solar nebula. Investigations conducted on CO chondrules, CM chondrites, the CV chondrite Allende, and the ungrouped carbonaceous chondrite WIS 91600 collectively indicate that, beyond 3 au, the solar nebula field strength ranged from 106^{+88}_{-18} μT to 4.4 ± 2.8 μT between 2.2

* Corresponding author.
E-mail address: cmaurel@cerege.fr (C. Maurel).

https://doi.org/10.1016/j.epsl.2023.118559
Received 5 October 2023; Received in revised form 20 December 2023; Accepted 21 December 2023
Available online 9 January 2024

± 0.8 and ~4 ± 1 Myr after CAI formation (Borlina et al., 2021; Bryson et al., 2020a; Cournède et al., 2015; Fu et al., 2021). On the other hand, paleointensities derived from CR chondrules, CO chondrites, the CV chondrite Kaba, and the ungrouped carbonaceous chondrite Tagish Lake are all compatible with a null magnetic field, for a period ranging between ~3 and ~5 Myr after CAI formation (Borlina et al., 2022; Bryson et al., 2020b; Fu et al., 2020; Gattacceca et al., 2016).

Magnetic fields in protoplanetary disks likely play a crucial role in the planetary accretion process. They can enhance turbulence and angular momentum transport in the disk, directly acting upon the motion and concentration of solids (Bai, 2017; Béthune et al., 2017). Extraterrestrial samples that experienced thermal metamorphism and/or aqueous alteration within the lifetime of the solar nebula may provide records of our own protoplanetary disk field, which are essential to advance our understanding of planetary formation (Weiss et al., 2021). However, finding samples exempt from terrestrial alteration or magnetic contamination (including the acquistion of a viscous remanent magnetization in the geomagnetic field) is challenging. In this regard, samples returned from asteroid Ryugu are ideal candidates to search for a paleomagnetic record of the solar nebula field.

Furthermore, Ryugu is only the second celestial body, after the Moon, for which we can confront asteroidal magnetometry data to natural remanent magnetization (NRM) measurements conducted on returned samples. In contrast to the Moon (Hood et al., 1981), however, the magnetometer on board the lander MASCOT (part of the Hayabusa 2 payload) did not measure any detectable magnetization at the surface of the asteroid (Herčik et al., 2020). The returned samples make it possible to test two contrasting hypotheses: (i) Ryugu's parent body experienced a very weak or null magnetic field during aqueous alteration, resulting in a magnetization too weak to be detected by the magnetometer, and (ii) Ryugu's parent body experienced a substantial magnetic field during aqueous alteration, but the resulting magnetization was randomized during regolith formation at a spatial scale smaller than the cm-scale resolvable by the magnetometer (Herčik et al., 2020). Testing these hypotheses will advance our understanding of the magnetization of celestial bodies, in the perspective of future missions with magnetometry experiments like the NASA Psyche mission (Weiss et al., 2023).

Ryugu samples contain ~6 vol.% of magnetite (mainly in the form of framboids, and plaquettes) and ~4 vol.% of pyrrhotite (Nakamura et al., 2022). If magnetite and pyrrhotite crystallized in the presence of a magnetic field, they may have acquired a chemical remanent magnetization (CRM) reflecting the intensity of this field. A CRM is acquired when magnetic minerals grow in field beyond their blocking volume (i.e., minimum volume required for a ferromagnetic mineral to acquire a remanent magnetization; Dunlop and Özdemir, 1997). Unlike a thermoremanent magnetization (TRM), acquired by a mineral upon cooling in field below its blocking temperature (i.e., the temperature below which a ferromagnetic mineral acquires a remanent magnetization), a CRM can be acquired at low temperature. Because Ryugu material has never been heated above ~100 °C (Yokoyama et al., 2023), a CRM would be the most likely magnetization acquisition mechanism for these samples.

Magnetite framboids form through the dissolution of antiferromagnetic hexagonal pyrrhotite during fluid-rock interactions (Zolensky et al., 2002). Unlike magnetite formed by pseudomorphic replacement of iron metal, magnetite framboids do not have a ferromagnetic precursor and do not inherit any remanence. They carry a single-phase CRM, which only reflects the magnetic environment at the acquisition epoch (Dunlop and Özdemir, 1997). Similarly, ferrimagnetic monoclinic pyrrhotite forms by replacement of non-magnetic troilite (Schrader et al., 2021) and may also acquire a single-phase CRM.

Electron holography conducted on Ryugu samples shows that magnetite framboids contain submicron grains in the magnetic single-vortex (SV) state (Kimura et al., 2023). SV particles of magnetite are known to be reliable magnetic recorders, capable of retaining their NRM over the age of the solar system (Nagy et al., 2017). The two μm-size pyrrhotite grains observed were in a multidomain magnetic state, i.e., non-ideal paleomagnetic recorders, but this may not be the case for all pyrrhotite grains in Ryugu samples.

Paleomagnetic measurements were conducted by Nakamura et al. (2022) on two samples from the two Hayabusa 2 sampling sites (A0026 and C0002–4-f, a fragment of C0002). These samples have a mass of 1.556 mg and 0.425 mg, respectively. The intrinsic magnetic properties of these two samples and four others (A0064-FC006, A0064-FO018, C0002–40, and C0023-FC009; no mass provided) were analyzed by Sato et al. (2022). The coercivity spectra of the samples are consistent with the presence of fine-grained magnetite and pyrrhotite, with average magnetic coercivities of 70 mT and 200 mT, respectively. The first-order reversal curve (FORC) diagram of A0064-FC006 displays features shared by other framboid-bearing meteorites (Sridhar et al., 2021). A0026 and C0002–4-f have NRMs of 3.99×10^{-2} A m^2 kg^{-1} and 2.14×10^{-2} A m^2 kg^{-1}. The alternating-field (AF) demagnetization of their NRMs exhibits a stable remanence component in the 10–30 mT and 0–20 mT coercivity ranges, respectively. This was interpreted as evidence for an ancient magnetizing field (the solar nebula field) with intensity between 41 and 390 μT (Sato et al., 2022).

Here, we present a new paleomagnetic study conducted on three Ryugu samples of 0.82, 0.97 and 21.87 mg. The difference in mass between the samples gives the opportunity to investigate the spatial scale of magnetization, and any effect due to the mineralogical heterogeneities that may exist among samples of 1 mg or less.

2. Material and method

We were granted by JAXA two particles (A0154 and C0005; supplementary Fig. S1) from the two Hayabusa 2 sampling sites. At the JAXA curation center, the particles were gently packed with quartz wool inside quartz containers sealed with parafilm. We provided the containers and wool, after confirming their very weak magnetic moment ($\leq 5 \times 10^{-11}$ A m^2). The containers were placed in mu-metal boxes to shield them from magnetic fields during shipment. Particle A0154 broke during transport into two samples (A0154-a and A0154-b) of 0.97 and 0.82 mg, respectively. These samples were kept 11 months in the mu-metal box inside a magnetically shielded room (total residual field ~1 nT, of the order of the interplanetary magnetic field) before conducting any measurement. We measured the NRM and low-field susceptibility of both A0154-a and A0154-b, before focusing on the largest fragment (A0154-a) for further paleomagnetic analyses. The NRM of C0005 was measured after 20 days in the same storage conditions as A0154. For comparison, we also analyzed a 47.1-mg sample of the CI chondrite Orgueil and a 1.1-mg sample of the CM2 chondrite Daoura 003, kept inside the shielded room (~500-nT residual field) for 18 years and 2 months, respectively.

All the experiments were conducted at the Centre Européen de la Recherche et de l'Enseignement des Géosciences de l'Environnement (CEREGE, France). The low-field susceptibility (χ_{LF}) and its anisotropy were measured with an Agico MFK1 with sensitivity of 5×10^{-13} m^3, operating at 200 A m^{-1} and 976 Hz. Calling $k_1 > k_2 > k_3$ the eigenvalues of the anisotropy of susceptibility matrix, the degree of anisotropy P is defined as k_1/k_3 and the shape parameter is defined as $[2\ln(k_2) - \ln(k_1) - \ln(k_3)]/[\ln(k_1) - \ln(k_3)]$ (Jelinek, 1981). The susceptibility was also measured at 15,616 Hz ($\chi_{15616Hz}$) to assess the quantity of superparamagnetic grains. Remanence measurements were conducted on a SQUID magnetometer (2 G Enterprises, model 755R, sensitivity 5×10^{-12} A m^2). Anhysteretic remanent magnetization (ARM) was imparted using an AGICO AF demagnetizer and anhysteretic magnetizer (model LDA5). Isothermal remanent magnetization (IRM) was imparted using the electromagnet of a LakeShore 8600 series vibrating sample magnetometer (VSM) once all other measurements were done. To avoid inflicting mechanical damage to the friable sample, the resulting IRM

was measured with the SQUID magnetometer and not with the VSM. AF demagnetization was conducted either with the LDA5 demagnetizer (for the NRM and ARM acquired in low DC bias fields) or using the automatic AF 3-axis degausser system attached to the SQUID magnetometer. When using the LDA5 demagnetizer, we followed a protocol that prevents the acquisition of gyroremanent magnetizations (GRM; Dunlop and Özdemir, 1997): (i) AF demagnetization along three orthogonal axes x, y, z and remanence measurement, (ii) AF demagnetization along x and remanence measurement, (iii) AF demagnetization along y and remanence measurement, and (iv) average of the three remanence measurements. None of the experiments were physically destructive to the samples (at the exception of their NRM), such that they will be sent back to JAXA in a pristine state for other studies.

The anisotropy of ARM was determined by acquiring and measuring an ARM (100-mT peak AC field, 250-μT bias field) along 18 directions (Jelinek, 1977). The definition of the degree of anisotropy and shape parameter is the same as for the anisotropy of susceptibility. The anisotropy matrix multiplies the directional remanence data to account for the effect of magnetic anisotropy. To characterize the significance of a NRM component over a given coercivity range, we used two parameters: MAD and DANG. The maximum angular deviation (MAD; (Kirschvink, 1980)) represents the variance of a vectorial dataset with respect to the direction of its first principal component. The deviation angle (DANG; (Tauxe and Staudigel, 2004)) is the angle between the direction of the first principal component and the vector connecting the center of mass of the dataset to the origin. We define a significant remanence component when MAD $< 25°$. A NRM component is considered origin trending if DANG $<$ MAD. When demagnetizing ARMs, we also computed the angular deviation δ of the component's direction (corrected for anisotropy effects) with respect to the ARM bias field direction. This parameter quantifies the directional fidelity of the ARM and relates to the capacity of a sample to acquire a remanence.

To estimate a paleointensity corresponding to a remanence component, we used the ARM and IRM normalization methods (Collinson and Stephenson, 1977; Gattacceca and Rochette, 2004), where the AF demagnetization of the NRM is followed by the AF demagnetization of an ARM or SIRM (saturation IRM acquired in a 2-T field). For an identified NRM component, the corresponding paleointensity (B_{paleo}) is estimated using Eq. (1a)-(1b):

$$B_{\text{paleo}} = \frac{B_{\text{ARM}}}{f}\frac{d\text{NRM}}{d\text{ARM}} \tag{1a}$$

$$B_{\text{paleo}} = a\frac{d\text{NRM}}{d\text{IRM}} \tag{1b}$$

In Eq. (1a)-b, B_{ARM} is the ARM bias field, NRM, ARM and IRM are the corresponding vectorial quantities lost with respect to the first demagnetization step of the selected component. The factors f and a are determined empirically and depend on the nature of the NRM (e.g., CRM or TRM) and of the remanence carriers. In the case of a single-phase CRM carried by magnetite, f and a follow lognormal distributions: $f = \text{lognorm}(\mu = -0.015, \sigma^2 = 0.35)$ and $a = \text{lognorm}(\mu = 8.09, \sigma^2 = 0.40)$. The corresponding geometric means of f and a are 0.99 and 3260 μT, respectively (Maurel and Gattacceca, 2023). Accounting for the rotation of Ryugu's parent body, B_{paleo} represents the projection of the magnetizing field vector onto the direction of the parent body's spin axis. The uncertainty resulting from this unknown direction is quantified by assuming a uniform probability distribution of spin axis orientations on the sphere, which yields an average multiplication factor of 2 for the paleointensity estimates (Fu et al., 2014).

3. Results

3.1. Intrinsic magnetic properties

Intrinsic magnetic properties are summarized in Table 1. Data acquired on the larger sample C0005 are probably more representative of the bulk Ryugu material. We measure a mass-weighted average χ_{LF} and saturation remanent magnetization (M_{rs}) of 1.02×10^{-4} m^3 kg^{-1} and 1.19 A m^2 kg^{-1}, respectively. The χ_{LF} and M_{rs} of A0154-a and A0154-b are 50% lower than the mass-weighted average, and their $M_{\text{rs}}/\chi_{\text{LF}}$ ratio, which depends on the assemblage of magnetic minerals but not on their total concentration, is 30% and 10% higher than the mass-weighted average, respectively. As could be anticipated, this reflects a heterogenous distribution of the magnetic minerals at the mg scale.

For C0005, we find $(\chi_{976\text{Hz}} - \chi_{15616\text{Hz}})/\chi_{976\text{Hz}} = 0.34\%$, indicating a negligible amount of superparamagnetic minerals in the sample. C0005 has a degree of anisotropy of susceptibility P of 1.11 and a shape factor T of 0.52 (oblate). In comparison, Orgueil has a degree of anisotropy of susceptibility of 1.03. The anisotropy of ARM measured on sample C0005 (resp. A0154-a) indicate a degree of anisotropy P of 1.28 (resp. 1.26) and a shape factor T of 0.027 (resp. −0.27).

The derivative of the IRM acquisition curve is relatively noisy. Because we had to move the samples from the VSM electromagnet to the SQUID magnetometer and back, this is likely due to the positioning error (in the VSM and the magnetometer) and the delay between IRM acquisition and measurement. Despite this, the derived coercivity spectrum (Fig. 1) is analogous to that of Sato et al. (2022) with two dominant populations of grains with average coercivities of 50 mT and 175 mT. The medium-coercivity population is consistent with the presence of SV magnetite grains (e.g., in the framboids). The high-coercivity population is consistent with the presence of pyrrhotite with grain size below ~2 μm (i.e., in the single domain magnetic state; Dekkers, 1988). This suggests that the electron holography measurements, showing only multidomain pyrrhotite, may not have captured the full pyrrhotite grain size distribution (Kimura et al., 2023). The ratio between an IRM given at 2T and −300 mT (S_{-300} ratio) of C0005 is −0.85, also consistent with the presence of a significant amount of high-coercivity pyrrhotite grains (Stober and Thompson, 1979).

3.2. NRM measurement and demagnetization

NRM intensities and demagnetization data are given in Tables 1-2. For A0154-a and A0154-b, we measured NRM intensities of 8.16×10^{-4} A m^2 kg^{-1} and 1.11×10^{-3} A m^2 kg^{-1}, respectively, after 11 months of storage in a ~1-nT field. C0005 had a NRM of 2.89×10^{-4} A m^2 kg^{-1} after 20 days in a ~1-nT field. The NRM demagnetizations of samples A0154-a and C0005 exhibit a poorly defined low-coercivity component up to ~8 mT (Table 2). The behavior of the NRM becomes erratic at higher AF steps up to 100 mT (or 200 mT for C0005; Fig. 2a-b), such that no significant component can be identified between 10 and 100 mT (MAD $> 25°$; Table 2). For both samples, the NRM intensity barely decreases upon AF demagnetization (Fig. 2e-f). A0154-a is also visibly acquiring spurious magnetizations as AF intensity increases (Fig. 2b). This demagnetization behavior is not due to instrumental noise of the SQUID magnetometer, which remained below 5×10^{-12} A m^2 throughout the experiment.

For comparison, the NRM demagnetization of Orgueil exhibits a non-origin-trending, low-coercivity component between 0 and 12 mT (MAD $< 25°$; Fig. 2c; Table 2). At higher AF steps (12–100 mT), the behavior becomes erratic with no identifiable component. Unlike Ryugu samples, the NRM intensity of Orgueil overall decreases up to 100 mT, but the sample also acquires spurious magnetizations above 12 mT (Fig. 2g). Overall, C0005, A0154-a and Orgueil share a similar NRM demagnetization behavior. The erratic NRM demagnetization pattern of A0154-a is not attributable to the small sample mass, as illustrated by the NRM demagnetization of a 1.1-mg sample of Daoura 003 (CM2 chondrite),

Table 1
NRM and intrinsic magnetic properties of A0154-a, A0154-b, C0005, Orgueil, Daoura 003 and Tagish Lake. Data acquired by Sato et al. (2022) on samples A0026 and C0002–4-f are also shown. Columns 2 to 5 show the mass, NRM, low-field susceptibility (χ_{LF}) and saturation remanent magnetization (M_{rs}). Columns 6 and 7 show the ratios NRM/χ_{LF} and NRM/M_{rs}. Columns 8 and 9 show the degree of anisotropy of magnetic susceptibility (P_{AMS}) and associated shape factor (T_{AMS}). Columns 10 and 11 show the degree of anisotropy of anhysteretic remanent magnetization (P_{AARM}) and associated shape factor (T_{AARM}). The susceptibility of Tagish Lake was measured for this study on a 5.51-g sample. The NRM and M_{rs} are mass-weighted averages. NRM intensities were measured for this study on nine samples with total mass of 12.55 g, including samples of 5.71, 5.51 and 1.01 g. M_{rs} values were measured on six samples between 8 and 38 g (Bryson et al., 2020b; Gattacceca and Rochette, 2004; Thorpe et al., 2002).

							AMS		AARM	
Sample	Mass (mg)	NRM (A m2 kg−1)	χ_{LF} (m3 kg−1)	Mrs (A m2 kg−1)	NRM/χ_{LF} (A m − 1)	NRM /Mrs	P	T	P	T
A0154-a	0.97	8.16×10^{-4}	3.54×10^{-5}	0.54	23	1.5×10^{-3}	–	–	1.26	−0.27
A0154-b	0.82	1.11×10^{-3}	4.84×10^{-5}	0.61	23	1.8×10^{-3}	–	–	–	–
C0005	21.87	2.89×10^{-4}	1.07×10^{-4}	1.24	3	2.3×10^{-4}	1.11	0.55	1.28	0.03
Orgueil	47.1	1.12×10^{-4}	5.24×10^{-5}	0.87	2	1.3×10^{-4}	1.03	−0.16	–	–
Daoura 003	1.1	5.73×10^{-4}	2.07×10^{-5}	0.70	28	8.2×10^{-4}	–	–	–	–
Tagish Lake	*	2.34×10^{-4}	7.93×10^{-5}	0.53	3	4.4×10^{-4}	–	–	–	–
A0026	1.56	3.99×10^{-2}	7.88×10^{-5}	1.07	507	3.6×10^{-2}	–	–	–	–
C0002–4-f	0.43	2.14×10^{-2}	7.88×10^{-5}	1.01	271	2.1×10^{-2}	–	–	–	–

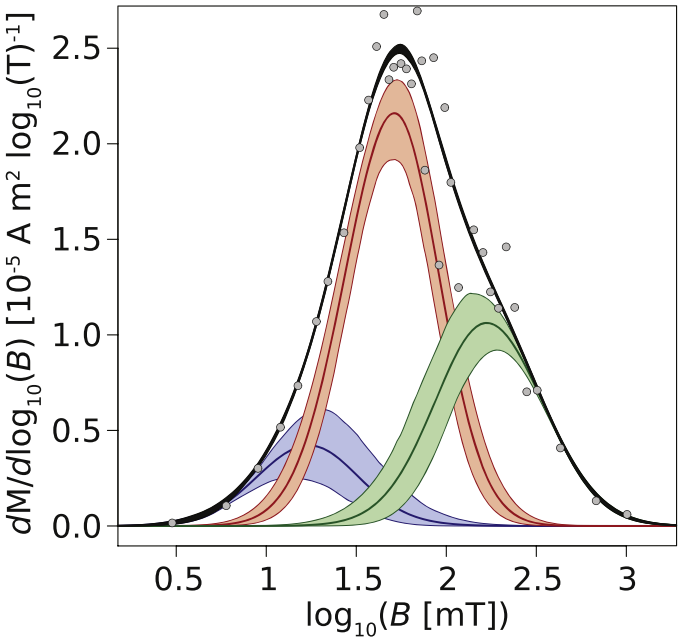

Fig. 1. Coercivity spectrum of sample C0005. Grey dots show the data, i.e., the derivative of the magnetic moment with respect to the $\log_{10}$ of the applied field. The black line shows the best fit to the data, obtained by summing the blue, red and green gaussian distributions representing different populations of grains. Shaded area show the 95% confidence intervals of each distribution. The blue, red and green distributions have average coercivities of 15, 50 and 175 mT, respectively. This figure was generated using the MaxUnmix software (Maxbauer et al., 2016).

where a clear high-coercivity component (24–100 mT, MAD = 7°; Table 2; Fig. 2d) can be identified.

3.3. ARM and IRM measurement and demagnetization

ARMs were applied in bias fields of 5, 10, 15, 20, 50, 100 and 200 μT. Considering the erratic demagnetization pattern of the NRM well below 100 mT, we used a peak AC field of 100 mT. For bias fields ≤ 15 μT, the ARM acquired by C0005 exhibits a similar demagnetization behavior as the NRM: no component is identifiable in the 10–100 mT coercivity range (Table 2; Fig. 3d,e), the intensity barely decreases (Fig. 3a) and is poorly correlated with the bias field intensity (Fig. 3b,c). For bias fields of 20 and 50 μT, the ARM of C0005 exhibits a remanence component between 10 and 100 mT with MAD < 25° and δ = 22° and 5°, respectively (Table 2; Fig. 3a,d,e). For bias fields > 50 μT, the ARM demagnetizes monotonically up to 100 mT, with a well-defined component in the 10–100 mT coercivity range aligned with the bias field (Table 2; Fig. 3d-e). The demagnetization patterns of ARMs imparted to Orgueil are similar to Ryugu samples, whereas an ARM with a 5-μT bias field imparted to Daoura 003 demagnetizes with a MAD of 14° and δ of 7° in the 10–100 mT coercivity range (Table 2).

3.4. Paleointensities

The REM' for C0005 (i.e., the slope of the NRM lost at each AF step normalized by the IRM lost at the same AF steps; Gattacceca and Rochette, 2004) increases in the 10–100 mT coercivity range (Fig. 4a). This can be attributed to the acquisition of spurious magnetizations during AF demagnetization of the NRM. Moreover, the slope of the NRM lost versus ARM lost (200-μT bias field) or IRM lost is indistinguishable from zero (Fig. 4b-c). These two paleointensity determination methods therefore do not discriminate between the absence or presence of a weak magnetic field during the aqueous alteration of Ryugu's parent body.

To place an upper limit on the paleofield intensity, we use the ARM normalization method, but replace the NRM data by the ARM data obtained with different bias fields:

$$B_{est} = B_{bias} \frac{d\mathrm{ARM}_{B_{bias}}}{d\mathrm{ARM}_{200\mu T}} \quad (2)$$

In Eq. (2), $\mathrm{ARM}_{200\mu T}$ is the vectorial quantity lost during demagnetization over the 10–100 mT coercivity range after imparting an ARM with a 200-μT bias field, $\mathrm{ARM}_{B_{bias}}$ is the vectorial quantity lost during demagnetization over the same coercivity range after imparting an ARM with a bias field B_{bias}, and B_{est} is the estimate of B_{bias} that can be retrieved from the data. We define the maximum paleointensity recordable by C0005 as the minimum B_{bias} needed for the 95% confidence interval of B_{est} to contain B_{bias} but not zero. After calculating B_{est} for B_{bias} = 5, 10, 15, 20, 50, and 100 μT, we find that this condition is met for $B_{bias} \geq 20$ μT (Fig. 5; Table 2).

A different test consists in calculating the metrics $D = B_{est} - B_{bias}/B_{bias}$ and $E = \sigma_{est}/B_{bias}$, where σ_{est} is the 95% confidence on B_{est} (Bryson et al., 2017). Using the criteria proposed by Bryson et al. (2020b), the minimum field recordable by a sample is equal to B_{bias} when $E \leq 1$ if $D \geq 0$, or $E \leq 0.5$ if $D \leq 0$. For C0005, this condition is met for B_{bias}= 20 μT and higher (Table 2), consistent with our findings.

A final step consists in taking into account that Ryugu's NRM is most likely a CRM. We must therefore ponder the minimum B_{bias} with the empirical coefficient f (Eq. (1a)). Using the geometric mean f = 0.99 determined for single-phase CRMs acquired by magnetite (Maurel and Gattacceca, 2023), we obtain an upper limit on the paleofield intensity

Table 2
NRM and ARM demagnetization parameters for A0154-a, C0005, Orgueil and Daoura 003. Column 2 shows the sample mass. Column 3 shows the ARM bias field intensity (except for NRMs). Columns 4 and 5 show the coercivity range considered and corresponding number of data points. Columns 6 and 7 show the norm and direction of the "component" calculated for the coercivity range in column 4. Columns 8, 9 and 10 show the MAD, DANG (for NRMs) and δ (for ARMs) calculated for the coercivity range in column 4. Column 11 shows the 95% confidence interval (CI) on the recorded field intensity retrieved using the ARM normalization method. Column 12 shows the values of the D and E parameters proposed by Bryson et al. (2017) to quantify the ARM recording capacity of a sample.

Sample	Mass (mg)	ARM field (μT)	AF range (mT)	N	Comp. norm ($A\ m^2\ kg^{-1}$)	D, I (°)	MAD (°)	DANG (°)	δ (°)	95% CI intensity (μT)	D, E
A0154-a	0.97	NRM	0–8	8	1.18×10^{-4}	109, 27	31	59	–	–	–
			10–100	29	2.03×10^{-3}	128, 40	46	71			
C0005	21.87	NRM	0–8	8	8.46×10^{-5}	125, 15	26	50	–	–	–
			10–100	30	3.51×10^{-4}	159, −2	41	33		[−41, 33]	
Orgueil	47.1	NRM	0–12	12	8.09×10^{-5}	11, −38	25	76	–	–	–
			13–100	26	6.90×10^{-5}	15, 50	45	52			
Daoura 003	1.1	NRM	32–100	12	2.72×10^{-4}	107, −29	7	26	–	–	–
C0005	21.87	5	0–10	10	2.09×10^{-4}	307, 5	14	–	57	–	–
			11–100	30	5.38×10^{-4}	327, −1	43		38	[−7, 23]	0.6, 3.0
C0005	21.87	10	0–10	10	1.13×10^{-4}	34, −26	44	–	42	–	–
			11–100	30	7.69×10^{-4}	34, 39	41		44	[−3, 27]	0.20, 1.5
C0005	21.87	15	11–51	30	6.78×10^{-4}	68, 1	38	–	60	[−18, 39]	−0.25, 2.6
C0005	21.87	20	0–10	10	4.54×10^{-4}	38, 5	28	–	33	–	–
			11–100	30	1.68×10^{-3}	348, 18	21		22	[11, 51]	0.55, 1.0
C0005	21.87	50	0–10	10	8.99×10^{-4}	10, 8	10	–	6	–	–
			11–100	23	2.17×10^{-3}	9, 7	24		5	[21, 64]	−0.14, 0.4
C0005	21.87	100	0–10	10	1.93×10^{-3}	6,9	5	–	5	–	–
			11–100	12	4.90×10^{-3}	5, 6	8		2	[80, 140]	0.10, 0.3
C0005	21.87	200	0–10	10	3.47×10^{-3}	12, 5	6	–	7	–	–
			11–100	23	8.32×10^{-3}	8, 3	5		3		
Orgueil	47.1	10	10–100	19	9.63×10^{-5}	8, −6	42	–	10	–	–
Orgueil	47.1	20	10–80	17	2.68×10^{-4}	195, 16	24	–	23	–	–
Orgueil	47.1	200	10–100	19	2.97×10^{-3}	5, 5	3	–	7	–	–
Daoura 003	1.1	5	10–100	11	1.57×10^{-4}	5, −5	14	–	7	–	–

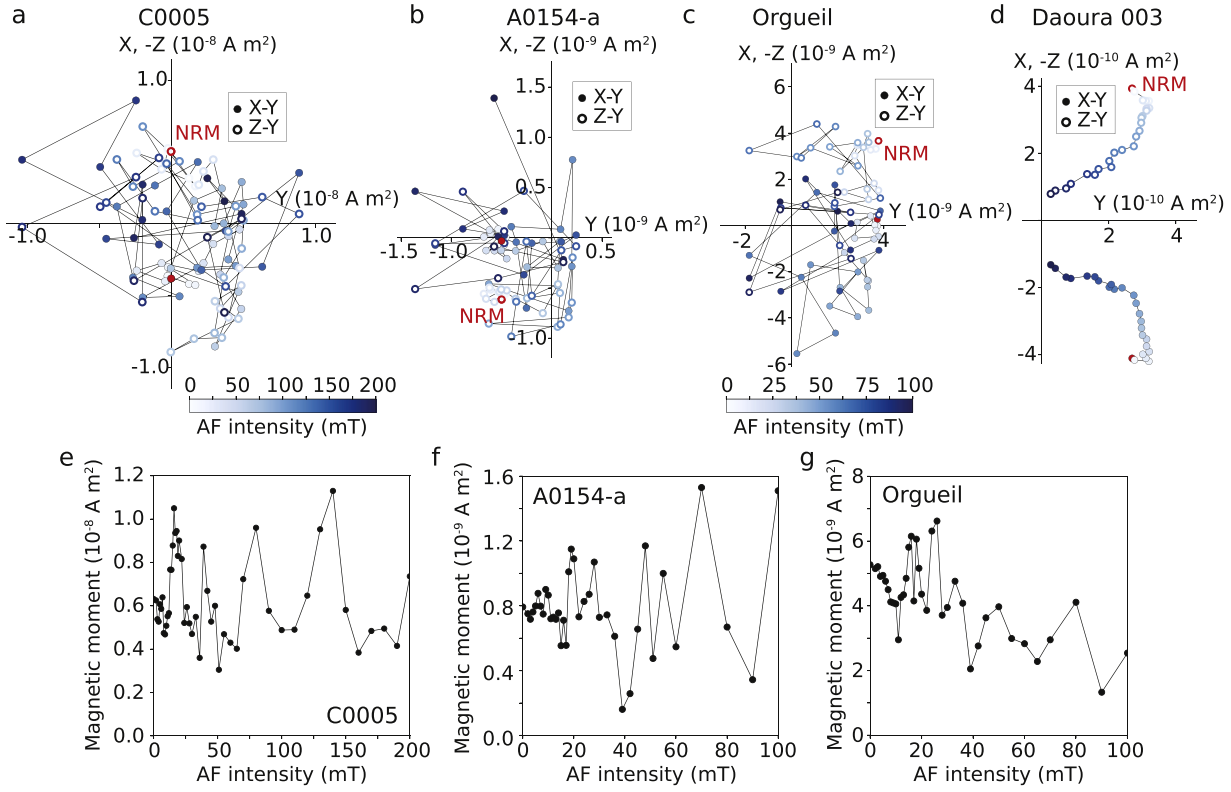

Fig. 2. (a) Orthogonal projection of the NRM of sample C0005 during stepwise AF demagnetization. Open and closed symbols show the projection onto the (y, z) and the (y, x) planes, respectively. The color scale indicates the AF intensity. The NRM is shown in red. (b) Same as (a) for sample A0154-a. (c) Same as (a) for the sample of the CI chondrite Orgueil. (d) Same as (a) for the CM2 chondrite Daoura 003. The color scale applies to (b-d). (e-g) NRM intensity as a function of AF intensity for C0005, A0154-a and Orgueil, respectively.

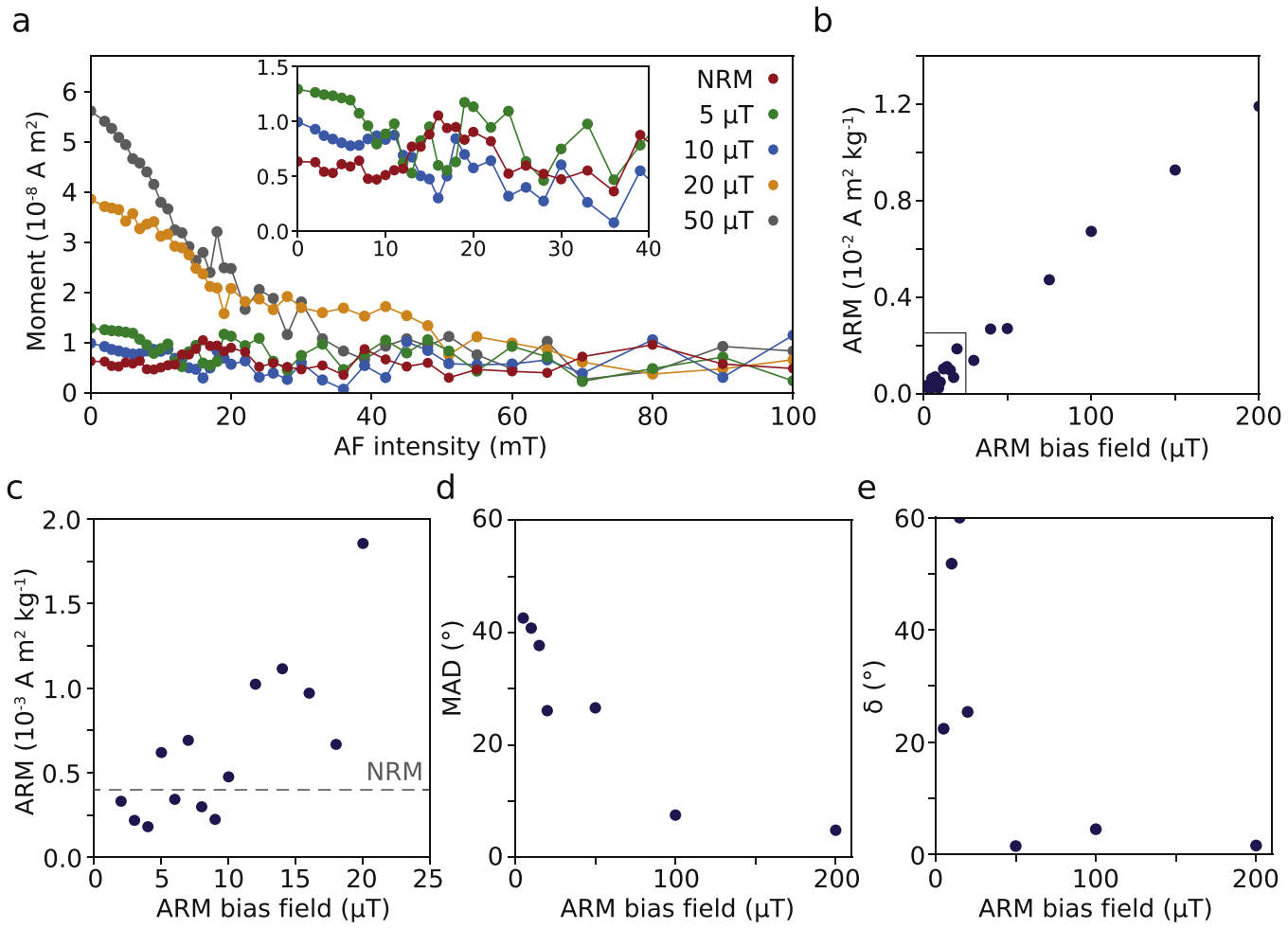

Fig. 3. (**a**) Magnetic moment of C0005 as a function of AF intensity during demagnetization of the NRM and ARMs acquired in bias fields between 5 and 50 μT. The inset is a zoomed-in view for AF intensities between 0 and 40 mT. (**b**) ARM intensity before demagnetization as a function of the ARM bias field intensity. For this figure, we measured the ARM acquired by C0005 in 21 different bias fields between 2 and 200 μT. (**c**) Zoomed-in view of the 0–25 μT ARM bias field range in (b). The dashed line shows the intensity of the NRM. (**d-e**) Maximum angular deviation (MAD) and angular deviation from the ARM bias field direction after anisotropy correction (δ) as a function of ARM bias field intensity for the 10–100 mT coercivity range.

experienced by C0005 of 20 μT. Taking into account the average correction resulting from the uncertainty on the direction of the parent body's spin axis, this upper limit becomes 40 μT.

An alternative approach is to consider our paleomagnetic data in light of those obtained on magnetite- and pyrrhotite-bearing meteorites that acquired a CRM during aqueous alteration of their parent body. These include the CM chondrites and Tagish Lake. The comparison with CM chondrites, however, is not appropriate given their differences in magnetic mineral assemblages (e.g., no magnetite framboids) and the fact that they exhibit a well-defined, high-coercivity NRM component (Cournède et al., 2015). On the other hand, Tagish Lake has a similar magnetic mineral assemblage as Ryugu samples (Zolensky et al., 2002), and exhibits an identical NRM demagnetization pattern. This meteorite experienced a field of < 1 μT, and possibly null, during the aqueous alteration of its parent body (Bryson et al., 2020b; upper limit recalculated using the empirical factor f given in Section 2). Comparing the NRM/M_{rs} ratio, which is a rough proxy for the paleointensity (Fuller and Cisowski, 1974; Wasilewski and Dickinson, 2000), of the two meteorites, we find that C0005 has a similar NRM/M_{rs} ratio as Tagish Lake, while A0154-a and A0154-b have ratios that are 3.5–4 times higher (Table 1). This suggests that the paleofield intensity recorded by Ryugu samples was much weaker than 40 μT, likely of a few μT at most, and possibly null.

4. Discussion

4.1. Implications of the results

Ryugu samples contain abundant magnetite framboids with single-vortex grains and fine-grained pyrrhotite, characterized as good magnetic recorders. Yet, C0005 cannot reliably acquire ARMs with bias fields < 20 μT. Orgueil, the closest meteorite analog to Ryugu samples, appears to have the same behavior. We suggest that both magnetostatic interactions between close-packed magnetic grains (like in magnetite framboids) and the anomalous behavior of pyrrhotite during ARM acquisition (Thomson, 1990) may act against the acquisition of low bias field ARMs. This would explain why the ARM normalization method does not provide an informative upper limit on the paleointensity for these specific samples. We note, however, that the poor ARM recording capacity of the samples does not necessarily reflect a poor CRM recording capacity, because the two mechanisms involve very different physical processes. For example, although pyrrhotite is a notoriously bad ARM recorder, it has been found to carry CRMs acquired in the geomagnetic field by sedimentary rocks (Evans et al., 2012), and in the weaker solar nebula field by CM chondrites (Cournède et al., 2015). To conclude, in the case of Ryugu samples, the method of normalization by M_{rs} provides a rough, yet robust estimate of the paleointensity as it

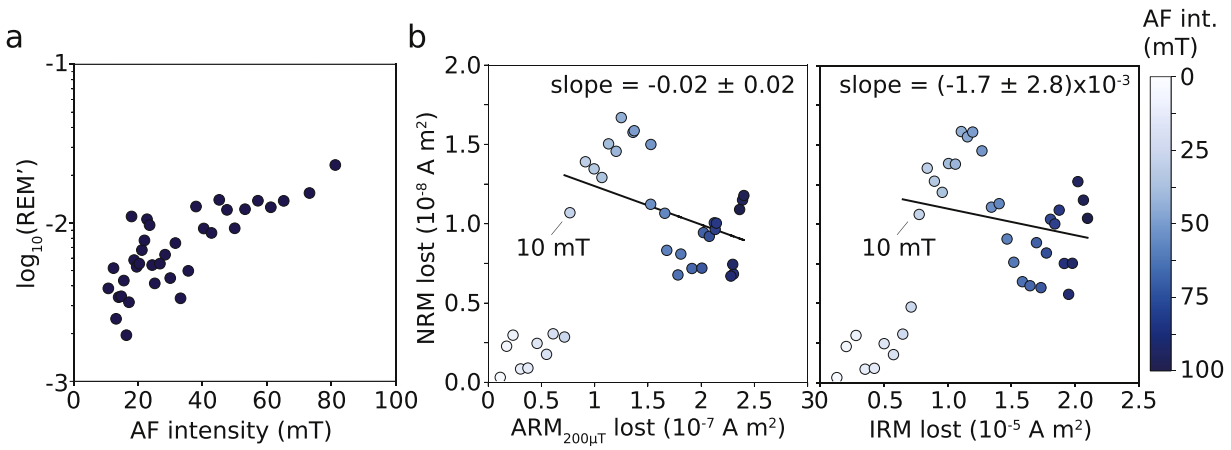

Fig. 4. (**a**) REM' (i.e., NRM lost normalized by IRM lost over the same AF step) as a function of AF intensity. (**b**) NRM lost as a function of $ARM_{200\mu T}$ (i.e., ARM acquired in a bias field of 200 μT) and IRM lost. The color scale indicates the AF intensity. The best linear fit to the data between 10 and 100 mT is shown, with its slope and two standard errors.

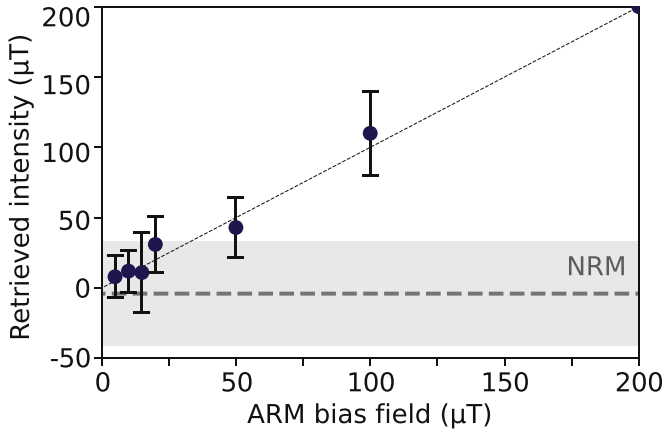

Fig. 5. Field intensity recorded by sample C0005 after applying an ARM with a bias field between 5 and 200 μT. This intensity is estimated using the ARM normalization method (Eq. (2)) for demagnetization data in the 10–100 mT coercivity range. The thin dashed line is the 1:1 line. Error bars represent the 95% confidence interval of the retrieved intensity. For reference, the horizontal dashed line and grey area show the mean and 95% confidence interval (-4 ± 37 μT) for the paleointensity estimated from the NRM demagnetization of C0005 (Eq. (1a)).

avoids the issues related to ARM acquisition (Gattacceca and Rochette, 2004).

The NRM intensity and NRM/M_{rs} ratio of C0005, A0154-a and A0154-b increase with decreasing sample mass (Table 1). Because at least some Ryugu samples are breccias (Nakamura et al., 2022), the random orientation of coherently magnetized clasts might explain this observation—with the caveat that part of the NRM may be a viscous remanence acquired in the geomagnetic field. The mass-normalized remanence of an ensemble of uniformly magnetized clasts that are randomly oriented decreases as $1/\sqrt{N}$, where N is the number of clasts of equal mass. As a result, the difference in NRM between C0005 and A0154 could be explained if C0005 was made of randomly oriented clasts of ~1 mg, which is broadly compatible with the clasts observed in some Ryugu samples (Nakamura et al., 2022). However, because 1 mg is approximately the mass of A0154-a and A0154-b, our data do not suggest that the absence of high-coercivity remanence can be explained by the random orientation of coherently magnetized clasts.

If Ryugu samples were aqueously altered in the presence of a field of a few μT, the prevalent sources for such a magnetizing field in the early solar system are (i) the solar nebula, (ii) a parent body dynamo powered by the advection of a liquid metallic core, and (iii) the early solar wind. Regarding (ii), thermal modeling of Ryugu's parent body suggests that this object did not experience temperatures above 120 °C through its entire volume (Nakamura et al., 2022), incompatible with the formation of a core and a dynamo activity. Regarding (iii), combined observations and models indicate that the early solar wind field did not exceed 300 nT, with a much lower average value given that its direction varied over timescales of a few hours (Oran et al., 2018). The most plausible source of magnetizing field for Ryugu samples would therefore be the solar nebula. This would imply that aqueous alteration on Ryugu's parent body occurred before its dissipation, i.e., before 5 Myr after CAI formation (Wang et al., 2017). In this case, the uncertainties on the age of aqueous alteration and on the paleointensity prevent us from estimating a minimum formation distance like it was done, for example, for WIS 91600 (Bryson et al., 2020a).

Alternatively, a very weak ($\lesssim$ 1 μT) or possibly null paleofield would be compatible with the aqueous alteration of Ryugu's parent body taking place either after the dissipation of the solar nebula ($\gtrsim$ 5 Myr after CAI formation), or at an earlier epoch but a large heliocentric distance (i.e., > 5 au, as suggested for Tagish Lake; Bryson et al., 2020b; recomputed by Maurel and Gattacceca, 2023). The discordant Mn-Cr ages of Ryugu's carbonates do not allow us to discriminate between these two possibilities (McCain et al., 2023; Yokoyama et al., 2023). Nevertheless, if Ryugu samples and Orgueil indeed share a similar geologic history, the hypothesis of an early and distant aqueous alteration of Ryugu's parent body is favored by the fact that (i) the magnetite extracted from Orgueil has a I-Xe age of 2.9 ± 0.3 Myr after CAI formation (Pravdivtseva et al., 2018), and (ii) the modeled age for the formation of the CI chondrite parent body is estimated at 3 Myr after CAI formation (Desch et al., 2018). This is consistent with other evidence in favor of a distant formation of Ryugu's parent body (e.g., Fe isotopic anomalies; Hopp et al., 2022), comparable to that of the CI chondrites, which may even have formed beyond 15 au (Desch et al., 2018).

4.2. Comparison with spacecraft data

The NRMs of C0005 and A0154 are 2 to 3 orders of magnitude higher than the upper limit on the magnetization of the top surface layer at the decimeter scale (10^{-6} A m^2 kg^{-1}) estimated at the MASCOT landing site (Herčik et al., 2020). A uniform surface magnetization of 3×10^{-4} A m^2 kg^{-1} such as that of C0005 (Table 1) would have been detected by the magnetometer. This confirms the findings of the magnetometry investigation team: 1) Ryugu's top surface layer was not magnetized after reaching its present-day rubble pile state, and 2) the non-detection of a

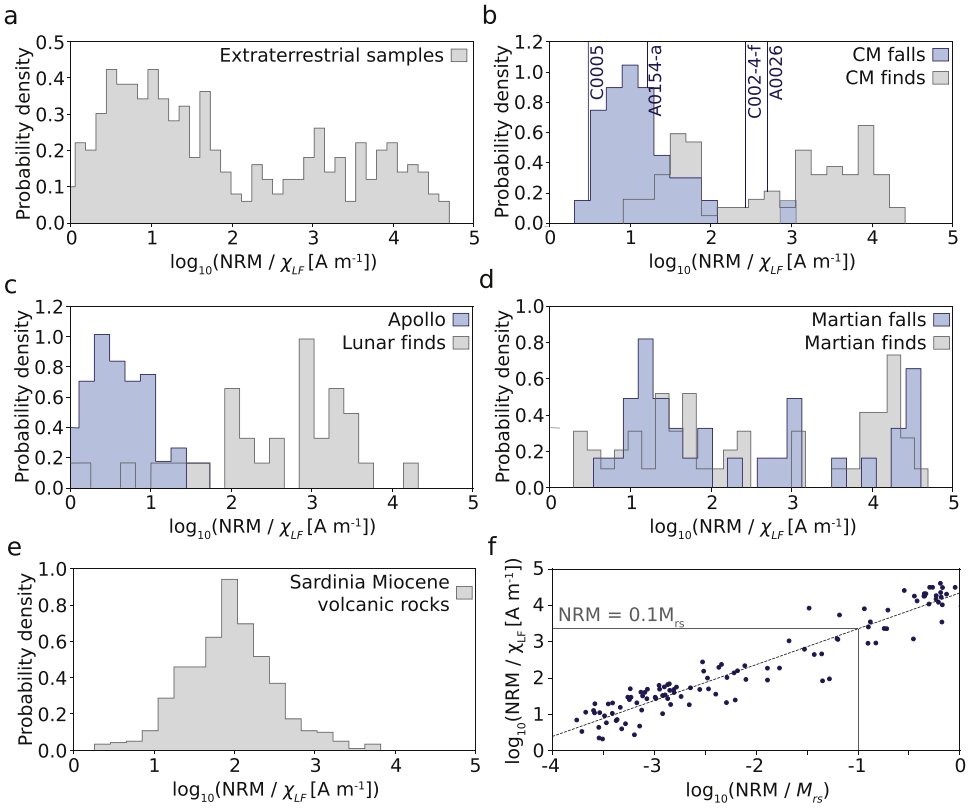

Fig. 6. (**a**) Histogram of measured NRM/χ_{LF} values for all extraterrestrial samples considered (CM chondrites, Lunar meteorites, Apollo samples and Martian meteorites; data compiled from Gattacceca and Rochette, 2004, Rochette et al., 2005, 2009, Cournède et al., 2015, Lepaulard et al., 2019, Bryson et al., 2023, and this study). (**b**) Measured NRM/χ_{LF} values for CM chondrites falls and finds. The vertical lines indicate the NRM/χ_{LF} values measured for Ryugu samples C0005, A0154-a, A0026 and C0002–4-f. (**c**) Measured NRM/χ_{LF} values for Apollo samples and Lunar meteorites finds. (**d**) Measured NRM/χ_{LF} values for Martian meteorites falls and finds. (**e**) Measured NRM/χ_{LF} values for Miocene volcanic rocks from Sardinia (Gattacceca et al., 2007). (**f**) NRM/χ_{LF} ratio as a function of NRM/M_{rs} ratio measured on the same sample, mixing all three meteorite groups.

surface magnetization is due to the random orientation of sub-centimeter magnetized regolith pebbles. In addition, MASCOT did not detect any magnetization when hitting a meter sized boulder (Herčik et al., 2020), consistent with a brecciated structure of the boulder at the cm scale or lower, as observed in some returned samples (Nakamura et al., 2022).

4.3. Comparison with published paleomagnetic data

The NRM intensity and the demagnetization pattern of C0005, A0154-a and A0154-b are very different from that of samples A0026 and C0002–4-f measured by Nakamura et al. (2022) and Sato et al. (2022), which have NRM intensities and NRM/M_{rs} ratios that are 1–2 orders of magnitude higher (Table 1). For A0026, the authors identify a NRM component between 12 and 32 mT, with a relatively constant REM' (average value of 3.2%), corresponding to a paleointensity of 106 μT using their estimated coefficient *a* of 3318 μT (Eq. (1b)). For C0002–4-f, the authors identify a NRM component between 2 and 24 mT, but the REM' decreases tenfold (from 12% to 1.2%) between 2 and 14 mT. Data corresponding to such a varying REM' should not be used for paleointensity estimation (Gattacceca and Rochette, 2004). If we restrict the component to the 14–24 mT coercivity range, the average paleointensity is 70 μT. Once multiplied by a factor of 2 to account for the uncertainty on the parent body's spin axis orientation, these paleointensities become 212 μT and 140 μT, respectively. These high paleointensity estimates are surprising compared to the data obtained from C0005 and A0154, which suggest a paleofield intensity of a few μT at most.

We argue that such large heterogeneities among samples that have similar masses (except C0005) and comparable intrinsic magnetic properties (χ_{LF}, M_{rs}, M_{rs}/χ_{LF}, coercivity spectrum) cannot arise naturally. Our interpretation is that the samples were magnetically contaminated prior to NRM demagnetization and that the derived paleointensities should not be interpreted as a record of the solar nebula field. This is strongly suggested by REM' values exceeding 10% (Verrier and Rochette, 2002) and decreasing in the 0–20 mT coercivity range. Given that C0005 and A0154 show no sign of remagnetization, this contamination did not take place during sampling, the journey back to Earth, or curation. We suspect the samples, once taken out of curation and prior to the paleomagnetic study, may have been exposed to artificial magnetic fields, possibly generated by other instruments. This contamination could result from the instantaneous exposure to strong fields (~20 mT) or latent exposure to fields of a few mT. In fact, experiments conducted on Apollo samples show that exposure to a field of 5 mT for 48 h can impart a stable remanence up to a coercivity of 30 mT (Tikoo and Jung, 2023).

4.4. Detection of artificial remagnetization of extraterrestrial samples

The apparent magnetic contamination of C0002–4-f and A0026 raises the question of whether it could have been detected prior to engaging into in-depth paleomagnetic experiments. In fact, the indicators commonly used to detect contamination, which include a curved demagnetization trajectory for the NRM or REM' values > 10% decreasing with increasing AF intensity, all require to demagnetize the NRM (Gattacceca and Rochette, 2004; Verrier and Rochette, 2002; Vervelidou et al., 2023).

We argue that the ratio NRM over low-field susceptibility (χ_{LF})—two quantities that can be measured without altering the NRM—is a first-

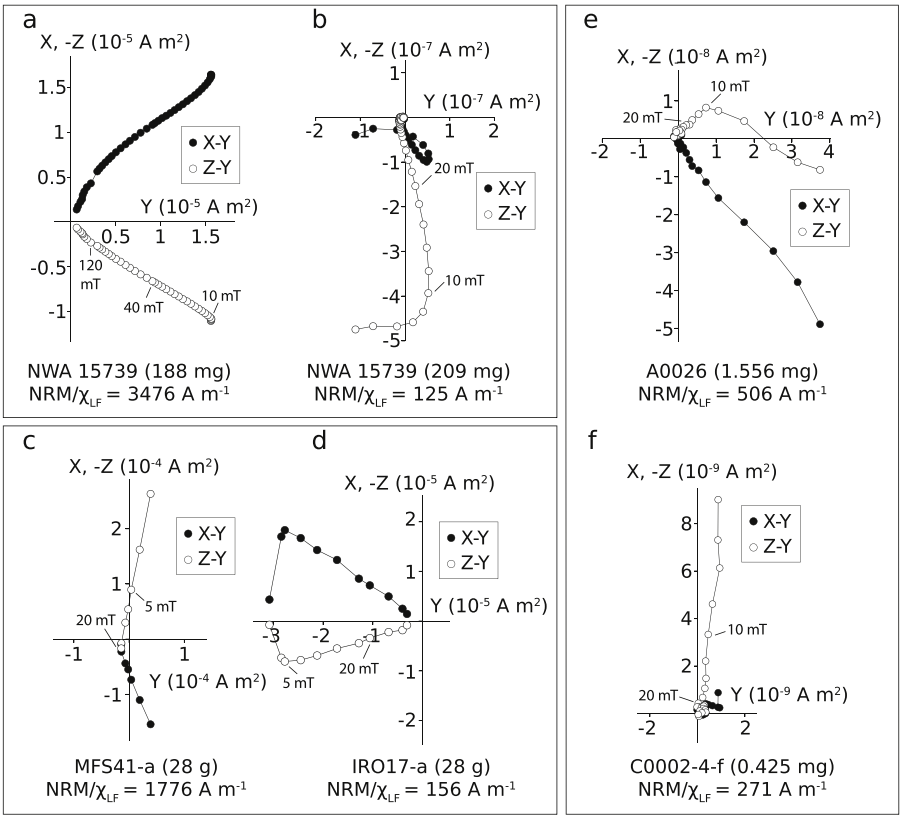

Fig. 7. (**a-b**) Orthogonal projections of the NRM during stepwise AF demagnetization for two samples of the CM chondrite NWA 15,739 with NRM/χ_{LF} ratios of 3476 and 125 A m^{-1} (measured for this study). Open and closed symbols show the projection onto two different planes. Some AF intensities are shown for reference. (**c-d**) same as (a) for two Miocene volcanic rocks from Sardinia with NRM/χ_{LF} ratios of 1776 and 156 A m^{-1} (adapted from Gattacceca et al., 2007) (**e-f**) Same as (a) for Ryugu samples A0026 and C0002–4-f with NRM/χ_{LF} ratios of 506 and 271 A m^{-1} (adapted from Sato et al., 2022).

order but efficient indicator of magnetic contamination. Much like NRM/M_{rs}, NRM/χ_{LF} is related to the paleointensity because χ_{LF} depends on the abundance of magnetic minerals in the rock. To illustrate this, we assembled a database of NRM/χ_{LF} ratios, measured for various extraterrestrial and terrestrial samples (supplementary Table S1): CM chondrites (falls and finds; Cournède et al., 2015; Bryson et al., 2023; this study), Martian meteorites (falls and finds; Rochette et al., 2005, 2009; this study), Lunar meteorites (only finds; no lunar meteorite fall has ever been collected; this study), Lunar samples returned by the Apollo missions (Lepaulard et al., 2019) and terrestrial Miocene volcanic rocks (Gattacceca et al., 2007). The meteorite susceptibilities were measured using an AGICO MFK1 operating at 200 A m^{-1} and 976 Hz or an AGICO KLY2 operating at 300 A m^{-1} and 920 Hz. The susceptibilities of Apollo samples were cross-calibrated against measurements conducted with an AGICO KLY2. The minor differences in operating field and frequency have a negligible effect on our analysis.

Taking all extraterrestrial samples together, the distribution of NRM/χ_{LF} ratios shows two distinct peaks, with average values near 10 A m^{-1} and 5000 A m^{-1}, respectively (Fig. 6a). Almost all CM falls have NRM/χ_{LF} < 100 A m^{-1} (Fig. 6b). For these CM falls, published data show that there is no characteristic curvature in the AF demagnetization of the NRMs, and that the integrated REM' values for the identified high-coercivity components are all < 1% (Cournède et al., 2015). We note that 14 out of the 15 CM falls that have NRM/χ_{LF} > 100 A m^{-1} are subsamples of the Winchcombe meteorite, which exhibit curved NRM demagnetizations that we suspect are due to a magnetic contamination (Bryson et al., 2023). All Apollo samples also have NRM/χ_{LF} < 100 A m^{-1} (Fig. 6c). The measurements were conducted on bulk samples with average mass of 500 g, never taken out of the Lunar Sample Laboratory Facility at NASA Johnson Space Center, such that magnetic contamination is unlikely. On the other hand, 70% of lunar meteorites (all finds) and 65% of CM finds have NRM/χ_{LF} > 100 A m^{-1} (with median values of 920 and 3500 A m^{-1}, respectively). This is consistent with the fact that meteorite finds are prone to contamination by magnets during collection, handling and testing by meteorite finders and dealers (Vervelidou et al., 2023). Contamination is even recognizable for CM finds with NRM/χ_{LF} ratios as low as 125 A m^{-1} (Fig. 7b). For Martian meteorites (Fig. 6d), the fraction of contaminated falls is larger than for CM chondrites. Almost all uncontaminated Martian finds were collected by the Antarctic search for meteorites (ANSMET) program, where the use of hand magnets is documented but remains a rare habit (Harvey et al., 2015).

Because both χ_{LF} and M_{rs} relate to the abundance of ferromagnetic minerals, NRM/χ_{LF} positively correlates with NRM/M_{rs} (Fig. 6f) and depends on the paleointensity. The NRM/χ_{LF} of a sample must therefore be interpreted in light of the distribution of NRM/χ_{LF} values for rocks with similar geologic history. It is illustrated by the fact that uncontaminated CM chondrites have a median ratio of 11 A m^{-1} and all those contaminated have NRM/χ_{LF} > 100 A m^{-1}, while uncontaminated terrestrial volcanic rocks have a median ratio of 90 A m^{-1} (Fig. 6e) and those with NRM/χ_{LF} > 1000 A m^{-1} (all sampled from cliffs at the top of mesa-like volcanic sequences) show evidence for remagnetization by lightning (Fig. 7c-d). For aqueously altered carbonaceous chondrites, a sample with NRM/χ_{LF} ratio between 100 and 200 A m^{-1} should already be treated with caution, whereas this threshold is closer to 1000 A m^{-1} for terrestrial volcanic rocks.

C0005, A0154-a and A0154-b have NRM/χ_{LF} ratios of 3, 23 and 23, respectively, while samples A0026 and C0002–4-f have NRM/χ_{LF} ratios of 506 and 271 (Table 1; Fig. 6b). Although A0026 and C0002–4-f do not exhibit a characteristic curved NRM demagnetization pattern (Fig. 7e-f), they both have REM' values starting at > 10% and decreasing down to 1–2% at AF steps of ~20 mT (Sato et al., 2022). The NRM/χ_{LF} ratio is

thus consistent with the conclusion that samples A0026 and C0002–4-f were partially remagnetized by artificial fields > mT, while samples C0005 and A0154 were not.

Measurements of NRM/χ_{LF} are fast and non-destructive, such that all samples considered for a paleomagnetic study could be screened before any further analyses. This naturally applies to returned samples, especially if other measurements are conducted prior to the paleomagnetic analyses, because many instruments (e.g., scanning electron microscopes) can generate magnetic fields. We note, however, that the NRM/χ_{LF} ratio does not account for the dependence of χ_{LF} on the nature and size of ferromagnetic grains, or for a partial magnetic overprint that may hide a residual, higher-coercivity NRM. Consequently, in the absence of alternative, the NRM of samples with high NRM/χ_{LF} ratios (e.g., 100–300 A m^{-1}) might still be worth analyzing.

5. Conclusion

We conducted a paleomagnetic investigation of three samples returned from asteroid Ryugu by the JAXA Hayabusa 2 mission (A0154-a, A0154-b and C0005, with masses of 0.97, 0.82 and 21.87 mg, respectively). Like other Ryugu samples, the magnetic properties of C0005 are compatible with the presence of fine-grained magnetite and pyrrhotite. C0005 and A0154-a do not exhibit a stable, origin trending magnetization upon AF demagnetization up to 200 mT. The ARM normalization paleointensity method is not adapted to Ryugu samples as it only provides an upper limit of 40 μT on the field strength experienced by Ryugu's parent body during its aqueous alteration. However, comparing the demagnetization pattern and NRM/M_{rs} of Ryugu samples with those of the ungrouped carbonaceous chondrite Tagish Lake, we conclude that this field was more likely of a few μT at most, and possibly very weak to null.

On the one hand, a paleointensity of a few μT would imply that the aqueous alteration of Ryugu's parent body occurred in the presence of the solar nebula field, earlier than ~5 Myr after CAI formation. On the other hand, a very weak ($\lesssim$ 1 μT) or null paleointensity would imply that the aqueous alteration took place either after the dissipation of the solar nebula, or at an earlier epoch and a large heliocentric distance (> 5 au). Refining the isotopic dating of aqueous alteration products is essential to discriminate between these hypotheses. Nonetheless, considering the age of magnetite in Orgueil and the similarities between Ryugu samples and CI chondrites, we favor the hypothesis of an early aqueous alteration at a large heliocentric distance.

The NRM intensities of C0005 and A0154 are two to three orders of magnitude higher than the detection limit of the magnetometer onboard the MASCOT lander, which did not measure any magnetization at the surface of Ryugu. This confirms that the asteroid was not remagnetized in its current state, and that the non-detection of a surface magnetization is likely due to the random orientation of sub-centimeter regolith pebbles.

Our results contrast with previous results indicating a ~140- to 212-μT paleofield (recomputed from Nakamura et al., 2022; Sato et al., 2022). Our alternative interpretation of these high paleointensities is that the samples used in these studies were contaminated by artificial magnetic fields (> mT), probably during experiments preceding the paleomagnetic investigations. We note, however, that because our samples show no evidence for partial remagnetization, no magnetic contamination took place *en masse* during sampling, storage in the spacecraft and curation.

Such a magnetic contamination could have been suspected after measuring the ratio of the NRM over low-field susceptibility (χ_{LF}). For instance, a NRM/χ_{LF} ratio > 100 A m^{-1} is a good indicator of probable remagnetization in hydrated carbonaceous chondrites. Measuring NRM/χ_{LF} is fast and non-destructive to the NRM. We recommend measuring this ratio before any detailed paleomagnetic investigation. Nevertheless, on returned samples, paleomagnetic measurements should as much as possible be conducted before other investigations.

CRediT authorship contribution statement

C. Maurel: Writing – original draft, Methodology, Investigation, Formal analysis, Data curation, Conceptualization. **J. Gattacceca:** Writing – review & editing, Methodology, Investigation, Formal analysis, Conceptualization. **M. Uehara:** Writing – review & editing, Methodology.

Declaration of competing interest

The authors declare that they have no known competing financial interests or personal relationships that could have appeared to influence the work reported in this paper.

Data availability

Data are available on the Zenodo repository with DOI: 10.5281/zenodo.8405497

Acknowledgements

We thank Prof Sonia Tikoo-Schantz, an anonymous reviewer and the editor for their constructive assessment of the manuscript. We are extremely grateful to JAXA for the loan of samples A0154 and C0005, and for the great care taken in handling and packing the samples for shipment to avoid magnetic contamination. We also thank the Museum National d'Histoire Naturelle de Paris (MNHN) for the loan of the Orgueil sample. The database of NRM/χ_{LF} ratios was constituted using data acquired on meteorite samples from the CEREGE meteorite collection, and loaned by private collectors and four institutions, which we thank: MNHN, Washington University, University of New Mexico and ANSMET. US Antarctic meteorite samples are recovered by the ANSMET program, which has been funded by NSF and NASA, and characterized and curated by the Department of Mineral Sciences of the Smithsonian Institution and Astromaterials Acquisition and Curation Office at NASA Johnson Space Center. We thank Dr François Demory and Gaëlle Ségué-Passama for assistance during the experiments. This project has received funding from the European Union's Horizon 2020 research and innovation programme under the Marie Skłodowska-Curie grant agreement No. 101027092. CM also acknowledges funding from the Centre National d'Etudes Spatiales (CNES).

Data are available on the Zenodo repository with DOI: 10.5281/zenodo.8405497.

Supplementary materials

Supplementary material associated with this article can be found, in the online version, at doi:10.1016/j.epsl.2023.118559.

References

Bai, X.N., 2017. Global simulations of the inner regions of protoplanetary disks with comprehensive disk microphysics. ApJ 845, 75.

Béthune, W., Lesur, G., Ferreira, J., 2017. Global simulations of protoplanetary disks with net magnetic flux - I. Non-ideal MHD case. Astron. Astrophys. 600, A75.

Borlina, C.S., Weiss, B.P., Bryson, J.F.J., Armitage, P.J., 2022. Lifetime of the outer solar system nebula from carbonaceous chondrites. J. Geophys. Res. Planets 127. https://doi.org/10.1029/2021je007139.

Borlina, C.S., Weiss, B.P., Bryson, J.F.J., Bai, X.N., Lima, E.A., Chatterjee, N., Mansbach, E.N., 2021. Paleomagnetic evidence for a disk substructure in the early solar system. Sci. Adv. 7, eabj6928.

Bryson, J.F.J., Nichols, C.I.O., Mac Niocaill, C., 2023. A unified intensity of the magnetic field in the protoplanetary disk from the Winchcombe meteorite. Meteorit. Planet. Sci. 1–22.

Bryson, J.F.J., Weiss, B.P., Biersteker, J.B., King, A.J., Russell, S.S., 2020a. Constraints on the distances and timescales of solid migration in the early solar system from meteorite magnetism. Astrophys J 896, 0–0.
Bryson, J.F.J., Weiss, B.P., Harrison, R.J., Herrero-Albillos, J., Kronast, F., 2017. Paleomagnetic evidence for dynamo activity driven by inward crystallisation of a metallic asteroid. Earth Planet. Sci. Lett. 472, 152–163.
Bryson, J.F.J., Weiss, B.P., Lima, E.A., Gattacceca, J., Cassata, W.S., 2020b. Evidence for asteroid scattering and distal solar system solids from meteorite paleomagnetism. Astrophys J 892, 126.
Collinson, D.W., Stephenson, A., 1977. Paleointensity determinations of lunar samples. Phys. Earth Planet. Inter. 13, 380–385.
Cournède, C., Gattacceca, J., Gounelle, M., Rochette, P., Weiss, B.P., Zanda, B., 2015. An early solar system magnetic field recorded in CM chondrites. Earth Planet. Sci. Lett. 410, 62–74.
Dekkers, M.J., 1988. Magnetic properties of natural pyrrhotite Part I: behaviour of initial susceptibility and saturation-magnetization-related rock-magnetic parameters in a grain-size dependent framework. Phys. Earth Planet. Inter. 52, 376–393.
Desch, S.J., Kalyaan, A., O'D. Alexander, C.M., 2018. The Effect of Jupiter's Formation on the Distribution of Refractory Elements and Inclusions in Meteorites. ApJS 238, 11.
Dunlop, D.J., Özdemir, Ö., 1997. Rock Magnetism: Fundamentals and Frontiers. Cambridge Univerty Press.
Evans, S.C., Douglas Elmore, R., Dennie, D., Dulin, S.A., 2012. Remagnetization of the Alamo breccia, Nevada, in: Elmore, R.D., Muxworthy, A.R., Aldana, M.M., Mena, M. (Eds.), Remagnetization and Chemical Alteration of Sedimentary Rocks. Geological Society, London, Special Publications 371, pp. 145–162.
Fu, R.R., Kehayias, P., Weiss, B.P., Schrader, D.L., Bai, X.N., Simon, J.B., 2020. Weak magnetic fields in the outer solar nebula recorded in CR chondrites. J. Geophys. Res. Planets 125. https://doi.org/10.1029/2019je006260.
Fu, R.R., Volk, M.W.R., Bilardello, D., Libourel, G., Lesur, G.R.J., Ben Dor, O., 2021. The fine-scale magnetic history of the Allende meteorite: implications for the structure of the solar nebula. AGU Adv. 2 https://doi.org/10.1029/2021av000486.
Fuller, M., Cisowski, S.M., 1974. Lunar Paleomagnetism. Rev. Geophys. 12, 23–70.
Gattacceca, J., Deino, A., Rizzo, R., Jones, D.S., Henry, B., Beaudoin, B., Vadeboin, F., 2007. Miocene rotation of Sardinia: New paleomagnetic and geochronological constraints and geodynamic implications. Earth Planet. Sci. Lett. 258, 359–377.
Gattacceca, J., Rochette, P., 2004. Toward a robust normalized magnetic paleointensity method applied to meteorites. Earth Planet. Sci. Lett. 227, 377–393.
Gattacceca, J., Weiss, B.P., Gounelle, M., 2016. New constraints on the magnetic history of the CV parent body and the solar nebula from the Kaba meteorite. Earth Planet. Sci. Lett. 455, 166–175.
Harvey, R.P., Schutt, J., Karner, J., 2015. Fieldwork methods of the US Antarctic search for meteorites program. In: Righter, K., Corrigan, C.M., Harvey, R.P., McCoy, T.J. (Eds.), 35 Seasons of U.S. Antarctic Meteorites: A Pictorial Guide to the Collection. AGU Special Publication, pp. 23–42.
Herčik, D., Auster, H.U., Constantinescu, D., Blum, J., Fornaçon, K.H., Fujimoto, M., Gebauer, K., Grundmann, J.T., Güttler, C., Hillenmaier, O., Ho, T.M., Hördt, A., Krause, C., Kührt, E., Lorda, L., Matsuoka, A., Motschmann, U., Moussi-Soffys, A., Richter, I., Sasaki, K., Scholten, F., Stoll, B., Weiss, B.P., Wolff, F., Glassmeier, K.H., 2020. Magnetic properties of asteroid (162173) ryugu. J. Geophys. Res. Planets 125. https://doi.org/10.1029/2019je006035.
Hood, L.L., Russel, C.T., Coleman, J., 1981. Contour maps of lunar remanent magnetic fields. J. Geophys. Res. 86, 1055–1069.
A. Hopp, T., Dauphas, N., Abe, Y., Aléon, J., Alexander, O.'.D., Amari, C.M., Amelin, S., Bajo, Y., Bizzarro, K.I., Bouvier, M., Carlson, R.W., Chaussidon, M., Choi, B.G., Davis, A.M., Di Rocco, T., Fujiya, W., Fukai, R., Gautam, I., Haba, M.K., Hibiya, Y., Hidaka, H., Homma, H., Hoppe, P., Huss, G.R., Ichida, K., Iizuka, T., Ireland, T.R., Ishikawa, A., Ito, M., Itoh, S., Kawasaki, N., Kita, N.T., Kitajima, K., Kleine, T., Komatani, S., Krot, A.N., Liu, M.C., Masuda, Y., McKeegan, K.D., Morita, M., Motomura, K., Moynier, F., Nakai, I., Nagashima, K., Nesvorný, D., Nguyen, A., Nittler, L., Onose, M., Pack, A., Park, C., Piani, L., Qin, L., Russell, S.S., Sakamoto, N., Schönbächler, M., Tafla, L., Tang, H., Terada, K., Terada, Y., Usui, T., Wada, S., Wadhwa, M., Walker, R.J., Yamashita, K., Yin, Q.Z., Yokoyama, T., Yoneda, S., Young, E.D., Yui, H., Zhang, A.C., Nakamura, T., Naraoka, H., Noguchi, T., Okazaki, R., Sakamoto, K., Yabuta, H., Abe, M., Miyazaki, A., Nakato, A., Nishimura, M., Okada, T., Yada, T., Yogata, K., Nakazawa, S., Saiki, T., Tanaka, S., Terui, F., Tsuda, Y., Watanabe, S.I., Yoshikawa, M., Tachibana, S., Yurimoto, H., 2022. Ryugu's nucleosynthetic heritage from the outskirts of the Solar System Sci. Adv. 8, eadd8141.
Jelinek, V., 1981. Characterization of the magnetic fabric of rocks. Tectonophysics 79, T63–T67.
Jelinek, V., 1977. The statistical theory of measuring anisotropy of magnetic susceptibility of rocks and its application. Geofyzika.
Kimura, Y., Kato, T., Tanigaki, T., Akashi, T., Kasai, H., Anada, S., Yoshida, R., Yamamoto, K., Nakamura, T., Sato, M., Amano, K., Kikuiri, M., Morita, T., Kagawa, E., Yada, T., Nishimura, M., Nakato, A., Miyazaki, A., Yogata, K., Abe, M., Okada, T., Usui, T., Yoshikawa, M., Saiki, T., Tanaka, S., Terui, F., Nakazawa, S., Yurimoto, H., Noguchi, T., Okazaki, R., Yabuta, H., Naraoka, H., Sakamoto, K., Watanabe, S.I., Tsuda, Y., Tachibana, S., 2023. Visualization of nanoscale magnetic domain states in the asteroid Ryugu. Sci. Rep. https://doi.org/10.1038/s41598-023-41242-x.
Kirschvink, J.L., 1980. The least-squares line and plane and the analysis of palaeomagnetic data. Geophys. J. Int. 62, 699–718.
Lepaulard, C., Gattacceca, J., Uehara, M., Rochette, P., Quesnel, Y., Macke, R.J., Kiefer, S.J.W., 2019. A survey of the natural remanent magnetization and magnetic susceptibility of Apollo whole rocks. Phys. Earth Planet. Inter. 290, 36–43.
Maurel, C., Gattacceca, J., 2023. Estimating paleointensities from chemical remanent magnetizations of magnetite using non-heating methods. J. Geophys. Res. Planets 128. https://doi.org/10.1029/2023je007779.
Maxbauer, D.P., Feinberg, J.M., Fox, D.L., 2016. MAX UnMix: a web application for unmixing magnetic coercivity distributions. Comput. Geosci. 95, 140–145.
McCain, K.A., Matsuda, N., Liu, M.C., McKeegan, K.D., Yamaguchi, A., Kimura, M., Tomioka, N., Ito, M., Imae, N., Uesugi, M., Shirai, N., Ohigashi, T., Greenwood, R.C., Uesugi, K., Nakato, A., Yogata, K., Yuzawa, H., Kodama, Y., Hirahara, K., Sakurai, I., Okada, I., Karouji, Y., Nakazawa, S., Okada, T., Saiki, T., Tanaka, S., Terui, F., Yoshikawa, M., Miyazaki, A., Nishimura, M., Yada, T., Abe, M., Usui, T., Watanabe, S.I., Tsuda, Y., 2023. Early fluid activity on Ryugu inferred by isotopic analyses of carbonates and magnetite. Nature Astronomy 7, 309–317.
Nagy, L., Williams, W., Muxworthy, A.R., Fabian, K., Almeida, T.P., Conbhuí, P.Ó., Shcherbakov, V.P., 2017. Stability of equidimensional pseudo-single-domain magnetite over billion-year timescales. Proc. Natl. Acad. Sci. U.S.A. 114, 10356–10360.
Nakamura, T., Matsumoto, M., Amano, K., Enokido, Y., Zolensky, M.E., Mikouchi, T., Genda, H., Tanaka, S., Zolotov, M.Y., Kurosawa, K., Wakita, S., Hyodo, R., Nagano, H., Nakashima, D., Takahashi, Y., Fujioka, Y., Kikuiri, M., Kagawa, E., Matsuoka, M., Brearley, A.J., Tsuchiyama, A., Uesugi, M., Matsuno, J., Kimura, Y., Sato, M., Milliken, R.E., Tatsumi, E., Sugita, S., Hiroi, T., Kitazato, K., Brownlee, D., Joswiak, D.J., Takahashi, M., Ninomiya, K., Takahashi, T., Osawa, T., Terada, K., Brenker, F.E., Tkalcec, B.J., Vincze, L., Brunetto, R., Aléon-Toppani, A., Chan, Q.H. S., Roskosz, M., Viennet, J.C., Beck, P., Alp, E.E., Michikami, T., Nagaashi, Y., Tsuji, T., Ino, Y., Martinez, J., Han, J., Dolocan, A., Bodnar, R.J., Tanaka, M., Yoshida, H., Sugiyama, K., King, A.J., Fukushi, K., Suga, H., Yamashita, S., Kawai, T., Inoue, K., Nakato, A., Noguchi, T., Vilas, F., Hendrix, A.R., Jaramillo-Correa, C., Domingue, D.L., Dominguez, G., Gainsforth, Z., Engrand, C., Duprat, J., Russell, S.S., Bonato, E., Ma, C., Kawamoto, T., Wada, T., Watanabe, S., Endo, R., Enju, S., Riu, L., Rubino, S., Tack, P., Takeshita, S., Takeichi, Y., Takeuchi, A., Takigawa, A., Takir, D., Tanigaki, T., Taniguchi, A., Tsukamoto, K., Yagi, T., Yamada, S., Yamamoto, K., Yamashita, Y., Yasutake, M., Uesugi, K., Umegaki, I., Chiu, I., Ishizaki, T., Okumura, S., Palomba, E., Pilorget, C., Potin, S.M., Alasli, A., Anada, S., Araki, Y., Sakatani, N., Schultz, C., Sekizawa, O., Sitzman, S.D., Sugiura, K., Sun, M., Dartois, E., De Pauw, E., Dionnet, Z., Djouadi, Z., Falkenberg, G., Fujita, R., Fukuma, T., Gearba, I.R., Hagiya, K., Hu, M.Y., Kato, T., Kawamura, T., Kimura, M., Kubo, M.K., Langenhorst, F., Lantz, C., Lavina, B., Lindner, M., Zhao, J., Vekemans, B., Baklouti, D., Bazi, B., Borondics, F., Nagasawa, S., Nishiyama, G., Nitta, K., Mathurin, J., Matsumoto, T., Mitsukawa, I., Miura, H., Miyake, A., Miyake, Y., Yurimoto, H., Okazaki, R., Yabuta, H., Naraoka, H., Sakamoto, K., Tachibana, S., Connolly, H.C., , Jr, Lauretta, D.S., Yoshitake, M., Yoshikawa, M., Yoshikawa, K., Yoshihara, K., Yokota, Y., Yogata, K., Yano, H., Yamamoto, Y., Yamamoto, D., Yamada, M., Yamada, T., Yada, T., Wada, K., Usui, T., Tsukizaki, R., Terui, F., Takeuchi, H., Takei, Y., Iwamae, A., Soejima, H., Shirai, K., Shimaki, Y., Senshu, H., Sawada, H., Saiki, T., Ozaki, M., Ono, G., Okada, T., Ogawa, N., Ogawa, K., Noguchi, R., Noda, H., Nishimura, M., Namiki, N., Nakazawa, S., Morota, T., Miyazaki, A., Miura, A., Mimasu, Y., Matsumoto, K., Kumagai, K., Kouyama, T., Kikuchi, S., Kawahara, K., Kameda, S., Iwata, T., Ishihara, Y., Ishiguro, M., Ikeda, H., Hosoda, S., Honda, R., Honda, C., Hitomi, Y., Hirata, N., Hirata, N., Hayashi, T., Hayakawa, M., Hatakeda, K., Furuya, S., Fukai, R., Fujii, A., Cho, Y., Arakawa, M., Abe, M., Watanabe, S., Tsuda, Y., 2022. Formation and evolution of carbonaceous asteroid Ryugu: direct evidence from returned samples. Science 379, eabn8671.
Oran, R., Weiss, B.P., Cohen, O., 2018. Were chondrites magnetized by the early solar wind? Earth Planet. Sci. Lett. 492, 222–231.
Pravdivtseva, O., Krot, A.N., Hohenberg, C.M., 2018. I-Xe dating of aqueous alteration in the CI chondrite Orgueil: I. Magnetite and ferromagnetic separates. Geochim. Cosmochim. Acta 227, 38–47.
Rochette, P., Gattacceca, J., Bourot-Denise, M., Consolmagno, G., Folco, L., Kouhout, T., Pesonen, L., Sagnotti, L., 2009. Magnetic classification of stony meteorites: 3. Achondrites. Met. Planet. Sci. 44, 405–427.
Rochette, P., Gattacceca, J., Chevrier, V., 2005. Matching Martian crustal magnetization and magnetic properties of Martian meteorites. Met. Planet. Sci. 40, 529–540.
Sato, M., Kimura, Y., Tanaka, S., Hatakeyama, T., Sugita, S., Nakamuna, T., Tachibana, S., Yurimoto, H., Noguchi, T., Okazaki, R., Yabuta, H., Naraoka, H., Sakamoto, K., Yada, T., Nishimura, M., Nakato, A., Miyazaki, A., Yogata, K., Abe, M., Okada, T., Usui, T., Yoshikawa, M., Saiki, T., Terui, F., Nakazawa, S., Watanabe, S.I., Tsuda, Y., 2022. Rock magnetic characterization of returned samples from asteroid (162173) ryugu: implications for paleomagnetic interpretation and paleointensity estimation. J. Geophys. Res. Planets 127 e2022JE007405.
Schrader, D.L., Davidson, J., McCoy, T.J., Zega, T.J., Russell, S.S., Domanik, K.J., King, A. J., 2021. The Fe/S ratio of pyrrhotite group sulfides in chondrites: an indicator of oxidation and implications for return samples from asteroids Ryugu and Bennu. Geochim. Cosmochim. Acta 303, 66–91.
Sridhar, S., Bryson, J.F.J., King, A.J., Harrison, R.J., 2021. Constraints on the ice composition of carbonaceous chondrites from their magnetic mineralogy. Earth Planet. Sci. Lett. 576, 117243.
Stober, J.C., Thompson, R., 1979. An investigation into the source of magnetic minerals in some Finnish lake sediments. Earth Planet. Sci. Lett. 45, 464–474.
Tauxe, L., Staudigel, H., 2004. Strength of the geomagnetic field in the cretaceous normal Superchron: new data from submarine basaltic glass of the Troodos ophiolite. Geochem. Geophys. Geosyst. 5 https://doi.org/10.1029/2003 gc000635.
Thomson, G.F., 1990. The anomalous demagnetization of pyrrhotite. Geophys. J. Int. 103, 425–430.
Thorpe, A.N., Senftle, F.E., Grant, J.R., 2002. Magnetic study of magnetite in the Tagish Lake meteorite. Meteorit. Planet. Sci. 37, 763–771.

Tikoo, S.M., Jung, J., 2023. Establishing a lunar origin for paleomagnetic records in Apollo samples. Geophys. Res. Lett. 50 https://doi.org/10.1029/2023 gl105152.
Verrier, V., Rochette, P., 2002. Estimating peak currents at ground lightning impacts using remanent magnetization. Geophys. Res. Lett. 29, 141–144.
Vervelidou, F., Weiss, B.P., Lagroix, F., 2023. Hand magnets and the destruction of ancient meteorite magnetism. J. Geophys. Res. Planets 128. https://doi.org/10.1029/2022je007464.
Wang, H., Weiss, B.P., Bai, X.N., Downey, B.G., Wang, Jun, Wang, Jiajun, Suavet, C., Fu, R.R., Zucolotto, M.E., 2017. Lifetime of the solar nebula constrained by meteorite paleomagnetism. Science 355, 623–627.
Wasilewski, P., Dickinson, T., 2000. Aspects of the validation of magnetic remanence in meteorites. Meteorit. Planet. Sci. 35, 537–544.
Watanabe, S., Hirabayashi, M., Hirata, N., Hirata, Na, Noguchi, R., Shimaki, Y., Ikeda, H., Tatsumi, E., Yoshikawa, M., Kikuchi, S., Yabuta, H., Nakamura, T., Tachibana, S., Ishihara, Y., Morota, T., Kitazato, K., Sakatani, N., Matsumoto, K., Wada, K., Senshu, H., Honda, C., Michikami, T., Takeuchi, H., Kouyama, T., Honda, R., Kameda, S., Fuse, T., Miyamoto, H., Komatsu, G., Sugita, S., Okada, T., Namiki, N., Arakawa, M., Ishiguro, M., Abe, M., Gaskell, R., Palmer, E., Barnouin, O.S., Michel, P., French, A.S., Mc Mahon, J.W., Scheeres, D.J., Abell, P.A., Yamamoto, Y., Tanaka, S., Shirai, K., Matsuoka, M., Yamada, M., Yokota, Y., Suzuki, H., Yoshioka, K., Cho, Y., Tanaka, S., Nishikawa, N., Sugiyama, T., Kikuchi, H., Hemmi, R., Yamaguchi, T., Ogawa, N., Ono, G., Mimasu, Y., Yoshikawa, K., Takahashi, T., Takei, Y., Fujii, A., Hirose, C., Iwata, T., Hayakawa, M., Hosoda, S., Mori, O., Sawada, H., Shimada, T., Soldini, S., Yano, H., Tsukizaki, R., Ozaki, M., Iijima, Y., Ogawa, K., Fujimoto, M., Ho, T.M., Moussi, A., Jaumann, R., Bibring, J.P., Krause, C., Terui, F., Saiki, T., Nakazawa, S., Tsuda, Y., 2019. Hayabusa2 arrives at the carbonaceous asteroid 162173 Ryugu—a spinning top–shaped rubble pile. Science 364, 268–272.
Weiss, B.P., Bai, X.N., Fu, R.R., 2021. History of the solar nebula from meteorite paleomagnetism. Sci Adv 7. https://doi.org/10.1126/sciadv.aba5967.
Weiss, B.P., Merayo, J.M.G., Ream, J.B., Oran, R., Brauer, P., Cochrane, C.J., Cloutier, K., Elkins-Tanton, L.T., Jørgensen, J.L., Maurel, C., Park, R.S., Polanskey, C.A., de Soria Santacruz-Pich, M., Raymond, C.A., Russell, C.T., Wenkert, D., Wieczorek, M.A., Zuber, M.T., 2023. The psyche magnetometry investigation. Space Sci. Rev. 219, 22.
Yada, T., Abe, M., Okada, T., Nakato, A., Yogata, K., Miyazaki, A., Hatakeda, K., Kumagai, K., Nishimura, M., Hitomi, Y., Soejima, H., Yoshitake, M., Iwamae, A., Furuya, S., Uesugi, M., Karouji, Y., Usui, T., Hayashi, T., Yamamoto, D., Fukai, R., Sugita, S., Cho, Y., Yumoto, K., Yabe, Y., Bibring, J.P., Pilorget, C., Hamm, V., Brunetto, R., Riu, L., Lourit, L., Loizeau, D., Lequertier, G., Moussi-Soffys, A., Tachibana, S., Sawada, H., Okazaki, R., Takano, Y., Sakamoto, K., Miura, Y.N., Yano, H., Ireland, T.R., Yamada, T., Fujimoto, M., Kitazato, K., Namiki, N., Arakawa, M., Hirata, Naru, Yurimoto, H., Nakamura, T., Noguchi, T., Yabuta, H., Naraoka, H., Ito, M., Nakamura, E., Uesugi, K., Kobayashi, K., Michikami, T., Kikuchi, H., Hirata, Naoyuki, Ishihara, Y., Matsumoto, K., Noda, H., Noguchi, R., Shimaki, Y., Shirai, K., Ogawa, K., Wada, K., Senshu, H., Yamamoto, Y., Morota, T., Honda, R., Honda, C., Yokota, Y., Matsuoka, M., Sakatani, N., Tatsumi, E., Miura, A., Yamada, M., Fujii, A., Hirose, C., Hosoda, S., Ikeda, H., Iwata, T., Kikuchi, S., Mimasu, Y., Mori, O., Ogawa, N., Ono, G., Shimada, T., Soldini, S., Takahashi, T., Takei, Y., Takeuchi, H., Tsukizaki, R., Yoshikawa, K., Terui, F., Nakazawa, S., Tanaka, S., Saiki, T., Yoshikawa, M., Watanabe, S.I., Tsuda, Y., 2021. Preliminary analysis of the Hayabusa2 samples returned from C-type asteroid Ryugu. Nature Astronomy 6, 214–220.
Yokoyama, T., Nagashima, K., Nakai, I., Young, E.D., Abe, Y., Aléon, J., Alexander, C.M. O., Amari, S., Amelin, Y., Bajo, K.I., Bizzarro, M., Bouvier, A., Carlson, R.W., Chaussidon, M., Choi, B.G., Dauphas, N., Davis, A.M., Rocco, T.D., Fujiya, W., Fukai, R., Gautam, I., Haba, M.K., Hibiya, Y., Hidaka, H., Homma, H., Hoppe, P., Huss, G.R., Ichida, K., Iizuka, T., Ireland, T.R., Ishikawa, A., Ito, M., Itoh, S., Kawasaki, N., Kita, N.T., Kitajima, K., Kleine, T., Komatani, S., Krot, A.N., Liu, M.C., Masuda, Y., McKeegan, K.D., Morita, M., Motomura, K., Moynier, F., Nguyen, A., Nittler, L., Onose, M., Pack, A., Park, C., Piani, L., Qin, L., Russell, S.S., Sakamoto, N., Schönbächler, M., Tafla, L., Tang, H., Terada, K., Terada, Y., Usui, T., Wada, S., Wadhwa, M., Walker, R.J., Yamashita, K., Yin, Q.Z., Yoneda, S., Yui, H., Zhang, A.C., Connolly, H.C., Lauretta, D.S., Nakamura, T., Naraoka, H., Noguchi, T., Okazaki, R., Sakamoto, K., Yabuta, H., Abe, M., Arakawa, M., Fujii, A., Hayakawa, M., Hirata, Naoyuki, Hirata, Naru, Honda, R., Honda, C., Hosoda, S., Iijima, Y.I., Ikeda, H., Ishiguro, M., Ishihara, Y., Iwata, T., Kawahara, K., Kikuchi, S., Kitazato, K., Matsumoto, K., Matsuoka, M., Michikami, T., Mimasu, Y., Miura, A., Morota, T., Nakazawa, S., Namiki, N., Noda, H., Noguchi, R., Ogawa, N., Ogawa, K., Okada, T., Okamoto, C., Ono, G., Ozaki, M., Saiki, T., Sakatani, N., Sawada, H., Senshu, H., Shimaki, Y., Shirai, K., Sugita, S., Takei, Y., Takeuchi, H., Tanaka, S., Tatsumi, E., Terui, F., Tsuda, Y., Tsukizaki, R., Wada, K., Watanabe, S.I., Yamada, M., Yamada, T., Yamamoto, Y., Yano, H., Yokota, Y., Yoshihara, K., Yoshikawa, M., Yoshikawa, K., Furuya, S., Hatakeda, K., Hayashi, T., Hitomi, Y., Kumagai, K., Miyazaki, A., Nakato, A., Nishimura, M., Soejima, H., Suzuki, A., Yada, T., Yamamoto, D., Yogata, K., Yoshitake, M., Tachibana, S., Yurimoto, H., 2023. Samples returned from the asteroid Ryugu are similar to Ivuna-type carbonaceous meteorites. Science 379, eabn7850.
Zolensky, M.E., Nakamura, K., Gounelle, M., Mikouchi, T., Kasama, T., Tachikawa, O., Tonui, E., 2002. Mineralogy of Tagish Lake: an ungrouped type 2 carbonaceous chondrite. Meteorit. Planet. Sci. 37, 737–761.